Experimental and Theoretical Study of the Infrared and Raman Spectra of a Substituted Sexithiophene in Five Oxidation States

J. Casado,[†] L. L. Miller,*[,‡,||] K. R. Mann,[‡] T. M. Pappenfus,[‡] V. Hernández,[§] and J. T. López Navarrete*[,§]

Departamento de Ingeniería Química, Química Física y Química Orgánica, Escuela Politécnica Superior, Universidad de Huelva, 21819-La Rábida, Huelva, Spain, Department of Chemistry, University of Minnesota, Minneapolis, Minnesota 55455, and Departamento de Química Física, Facultad de Ciencias, Universidad de Málaga, 29071-Málaga, Spain

Received: October 18, 2001; In Final Form: January 23, 2002

The infrared absorption and Raman scattering spectra recorded during the electrochemical oxidation of two sexithiophenes are reported. Using in situ spectroelectrochemical methods five oxidation states, neutral, radical cation, dication, radical trication, and tetracation of an α,α′-diphenyl sexithiophene, were studied. The experimental spectra are in agreement with the predictions of the effective conjugation coordinate theory and are in good accordance with theoretical density functional theory calculations.

I. Introduction

Linear π-conjugated polymers and oligomers are the focus of intense research efforts motivated by their unusual electronic properties, and by their potential applications for electronics and photonics.[1−3] Charged defects, in the form of radical cations, π-dimers, π-stacks, dications, radical anions, dianions, etc., play an important role in these materials.[4] In recent years, many papers devoted to longer oligomers, e.g., oligothiophenes and oligophenylene-vinylenes with 10−20 ring units, and to longer mixed oligomeric systems made with phenyl, thiophene, or pyrrole rings, have been presented.[5−7] The ability of small (2−6 rings) terminally capped thiophene oligomers to produce stable cation radicals and dications is well-known, but evidence of higher oxidation levels, even in longer oligomers, is relatively rare.[4,8] The first evidence of a trication species was seen by Parakka et al. for a heptamer containing four thiophene and three pyrrole rings.[9] Recently, Roncali and co-workers have observed that a 16-mer thienylene-vinylene molecule can be oxidized to the hexacation and even to the octacation in the case of the 20−22-mer oligomers.[6,10] These works have focused on the multielectronic processes that take place during the electrochemical oxidation of these macromolecules. The oxidized species have been mainly characterized by cyclic voltammetry and by UV−vis−NIR and EPR spectroscopies.

Very recently 3′,4′,3‴,4‴-tetrabutyl-5,5‴-dimethyl-2,2′:5′,2″:5″,2‴:5‴,2⁗:5⁗,2⁗′-sexithiophene (Me_2Bu_4SxT) and 3′,4′,3‴,4‴-tetrabutyl-5,5‴-diphenyl-2,2′:5′,2″:5″,2‴:5‴,2⁗:5⁗,2⁗′-sexithiophene (Ph_2Bu_4SxT) have been synthesized (Figure 1).[11] Figure 2 shows the cyclic voltammograms of Me_2Bu_4SxT and Ph_2Bu_4SxT. Unexpectedly, the phenyl end-capped sexithiophene showed not two, but four reversible one-electron oxidations. The electronic absorption spectra of the four electrochemically oxidized species are characterized by the presence of two new bands at 811 and at 1670 nm in the first oxidized species; in the second oxidized species an intense band at 1155 nm (with a shoulder at 1006 nm) is observed; the third electron extraction generates the appearance of a intense band at 1160 nm together with a medium intensity band at 999 nm, and a weak electronic absorption at 1790 nm. Finally, the highest oxidized species of Ph_2Bu_4SxT is characterized by two medium intensity bands at 966 and 864 nm.[11] Much as the electronic spectra show, more work is needed to understand the electronic structure and topology of the defects and to explain the influence of the phenyl end-caps and the butyl side-chains in the stabilization of these polycations.

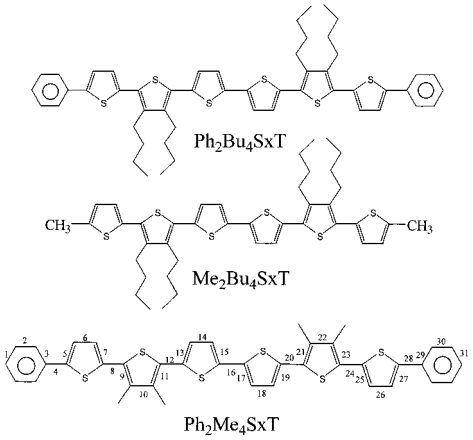

Figure 1. Chemical structure of the oligothiophenes studied in this work. Bond numbering of Ph_2Me_4SxT corresponds to that appearing in Figure 3.

Vibrational spectroscopy is one of the most important and promising tools for the characterization of conjugated oligomeric and polymeric materials in the neutral and oxidized state.[12,13] The combination of theoretical calculations with infrared and Raman spectroscopies provides invaluable structural information. The main objective of structural studies is the elucidation of the relationship between the electrical conduction phenomena and the structural modifications of the oligomer backbone. Since detailed information on bond lengths and bond angles for the oxidized species is difficultly accessible, the use of vibrational

* To whom correspondence should be addressed.
|| E-mail: lmiller@chem.umn.edu.
† Departamento de Ingeniería Química.
‡ Department of Chemistry.
§ Departamento de Química Física.

10.1021/jp0138678 CCC: $22.00
Published on Web 03/12/2002

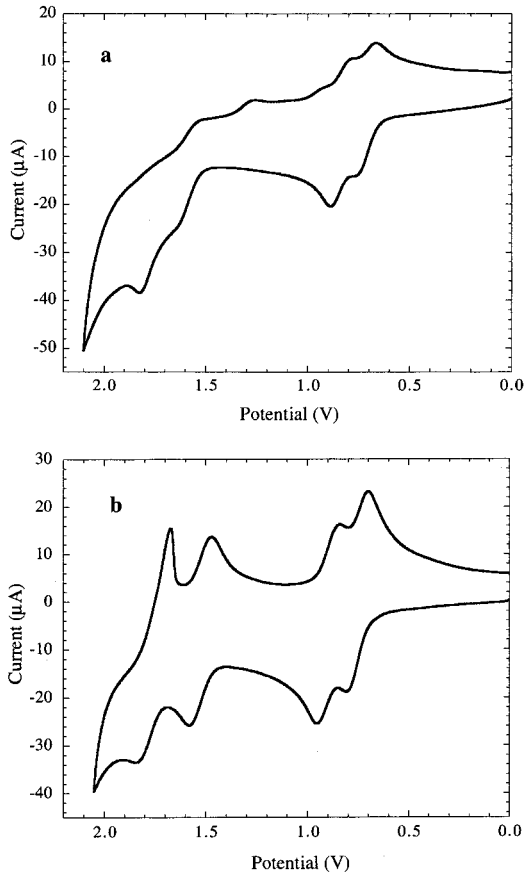

Figure 2. Cyclic voltammetry of (a) Me_2Bu_4SxT and of (b) Ph_2Bu_4SxT.[11]

spectroscopies and calculations becomes one of the most important tools to probe such modifications after chemical or electrochemical doping.[14−16]

In central papers for the current understanding of vibrational spectroscopy of conjugated molecules, Zerbi et al. introduced the concept of the effective conjugation coordinate (ECC).[17] In heteroaromatic systems, this collective coordinate may be viewed as the linear combination of ring C=C/C−C stretching coordinates which point in the direction from a benzenoid structure (usually the ground state) to a quinonoid structure (usually the first electronically excited state or the charged defect). This coordinate is involved in all the major vibrational spectroscopic aspects of polyconjugated molecules because it represents that coordinate which describes the important structure changes occurring upon chain elongation or upon oxidation or excitation. For example, due to the strong coupling between the ECC mode and the π-electron delocalization (*electron−phonon* coupling), the Raman band associated with the ECC mode is usually the most intense band in the Raman spectra of the conjugated molecules. In heteroaromatic systems, reversible oxidation processes generate quinonoid structures in the molecule. Thus, on going from the neutral to the oxidized species, the oligomer backbone changes from an heteroaromatic to a quinonoid structure. During this process, the double C=C ring bonds are weakened, while the single C−C intra and inter-ring bonds are strengthened. Therefore, compared to the neutral form, the molecular vibrations with a large content of ν(C=C) motions (mainly the ECC mode) show a frequency downshift of the associated band on going to the most oxidized species.

Current quantum chemical methods give reliable information about the molecular structure and the vibrational properties of the different classes of charged defects in doped polyconjugated molecules.[14−16] Density functional theory (DFT) is an efficient approach for adding electron correlation and its computational requirements are comparable to those of the Hartree−Fock (HF) method. DFT studies have proved very useful in the study of charged molecules or ions.[18,19] The spin-unrestricted DFT methods have been successfully applied to the study of the polaron to bipolaron transition in oligophenyls.[20] Thus, our theoretical approach is based on a DFT method to calculate the ground-state geometry as well as the vibrational frequencies and intensities for model oligothiophenes. DFT methods have been shown to provide accurate geometries and vibrational frequencies for conjugated oligomers. In particular, DFT calculated vibrational spectra usually do not require any rescaling of the frequecies prior to comparison with experiment, because electron correlation is explicitly taken into account.[21,22]

This paper describes the spectra of five species involved in the electrochemical oxidation of Ph_2Bu_4SxT. Band assignments are made by comparison to similar previously studied compounds. ECC theory is used to interpret changes in the Raman and infrared spectra in terms of a quinonoid structure growing at the expense of the benzenoid one and DFT theory gives Raman shifts and vibrational frequencies. To our knowledge, a comparison of theory and experiments of this type has not been made over this large range of oxidation states.

II. Experimental and Computational Methods

Raman experiments were carried out in a thin layer electrochemical cell using a 0.53 mM solution of the hexamers in 0.1 M $TBAPF_6/CH_2Cl_2$. An ITO electrode and a platinum electrode were used, respectively, as working and as auxiliary electrodes. All spectroelectrochemical measurements were carried out using an Ag wire as pseudo-reference electrode. IR experiments were carried out using a specular reflectance spectroelectrochemical cell.

FT-Raman spectra were measured using an FT-Raman accessory kit (FRA/106-S) of a Bruker Equinox 55 FT-IR interferometer. A continuous-wave Nd:YAG laser working at 1064 nm was employed for Raman excitation. A germanium detector operating at liquid nitrogen temperature was used. Raman scattering radiation was collected in a backscattering configuration with a standard spectral resolution of 4 cm^{-1}. To avoid possible damage of the sample upon laser radiation, the laser beam was loosely focused on the sample and its power was kept at a level lower than 30 mW. To avoid degradation processes in the sample, it was found that the average of 150 scans is the lowest acquisition scan number that guarantees the recording of a well-resolved Raman spectrum. A Nicolet 550 IR spectrometer equipped with a MCD detector was used for the IR measurements.

DFT calculations were carried out with the GAUSSIAN 98 program[23] using a SGI Origin 2000 supercomputer. Theoretical calculations were carried out on Ph_2Me_4SxT as a model molecule for Ph_2Bu_4SxT (see Figure 1 for chemical structures). The geometry optimizations are performed on isolated entities. The neutral, dication and tetracation molecules were treated as closed-shell (B3LYP procedure), while for the radical cation and the radical trication, open-shell systems, optimizations were carried out using wave functions spin unrestricted UB3LYP.[24] In several studies, it has been shown that B3LYP functional yields similar geometries for medium-sized molecules as MP2 calculations do with the same basis set.[25] Furthermore the DFT force fields calculated using the B3LYP functional yields infrared absorption spectra in good agreement with experiments.[26,27] The 3-21G* basis set has been used throughout this

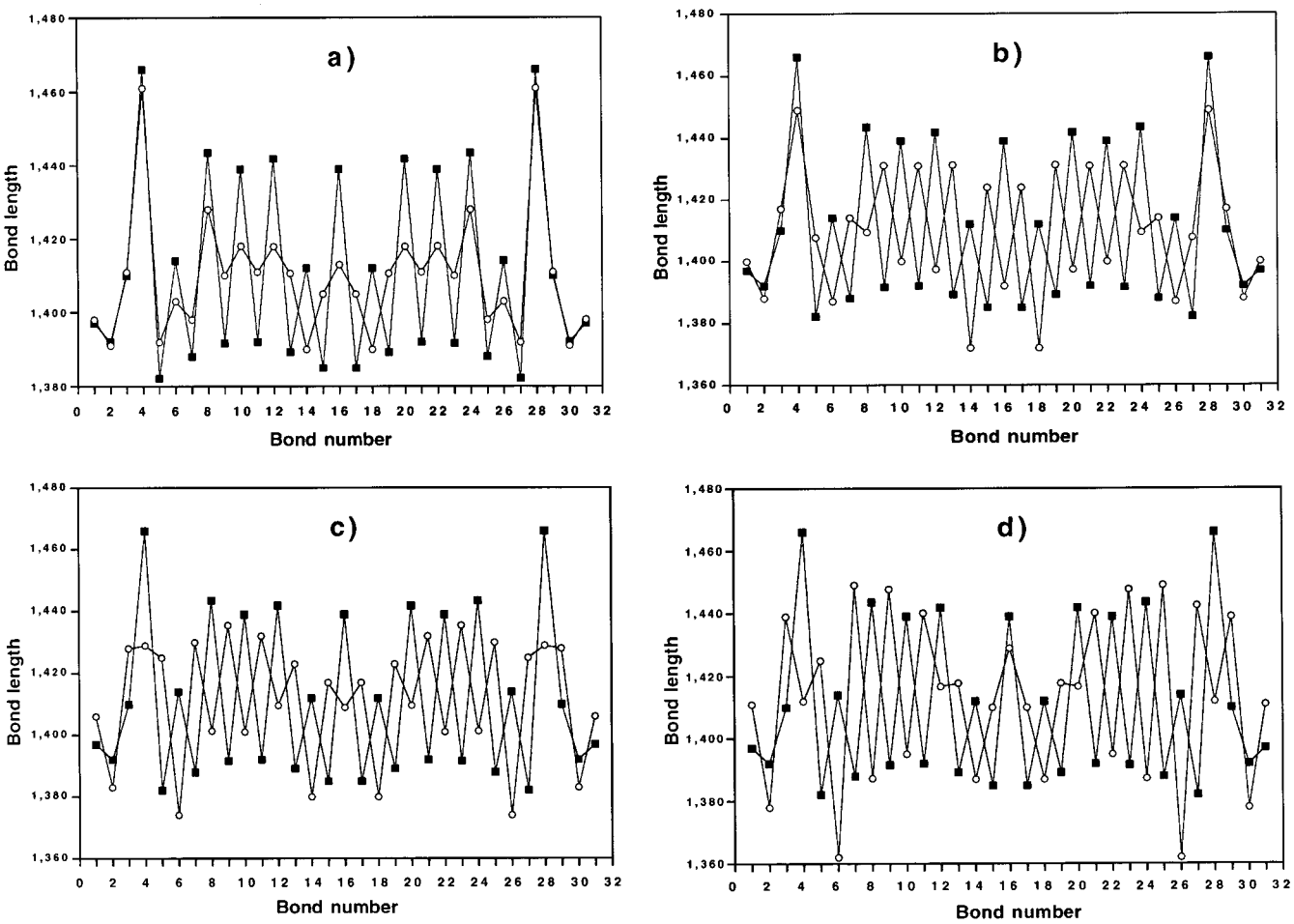

Figure 3. Optimized CC bond lengths of Ph_2Me_4SxT in neutral state (filled squares) and as (a) radical cation, (b) dication, (c) radical trication, and (d) tetracation (open circles). The B3LYP/3-21G* and UB3LYP/3-21G* methods have been used for the closed-shell and for the open-shell systems, respectively.

work as a compromise between accuracy and applicability to large molecules.[28] The structures of the neutral and ionized molecules were optimized under the following constraints: (a) all oligomers were kept planar and (b) only the all-anti conformations were treated throughout. No scale factors were used for calculations of vibrational frequencies. A zero energy Raman excitation line was assumed, so no resonance Raman effects are included.

III. Theoretical Results

The number as well as the size of the molecules treated in this work are too large to report in detail all the various equilibrium structures and charges, vibrational frequencies, infrared and Raman intensities, and the vibrational assignments. Instead, we restrict our discussion to the most important structural and vibrational spectroscopic features that help us to analyze the experimental data.

Figure 3 shows the evolution of the B3LYP/3-21G* calculated CC bond lengths of the molecular thiophene backbone for the neutral species, the radical cation, the dication, the radical trication, and the tetracation of Ph_2Me_4SxT. In the case of the neutral molecule (Figure 3a), the optimized geometric structure is calculated to be aromatic for both thiophene and benzene rings. Compared to the neutral, the geometric structure of the radical cation of Ph_2Me_4SxT (Figure 3a) shows a reversed bond-length alternation pattern in the two central thiophene rings: the bond lengths of the two inner thiophene rings (bond numbers 13, 15, 17, and 19 in Figure 1) increase by 0.02 Å, and the central inter-ring bond (bond number 16) shortens from 1.439 to 1.413 Å. Assuming that a pure aromatic polythiophene (PTh) has an inter-ring bond length of 1.47 Å (based on Badger's rule) and that corresponding value for the pure quinonoid PTh is 1.32 Å, a quinonoid character in the 2 central thiophene rings in $Ph_2Me_4SxT^{+\cdot}$ is apparent.[29]

For the optimized geometry of the $Ph_2Me_4SxT^{2+}$ (Figure 3b) and respect to the neutral form an average reversed bond-length alternation pattern of 0.04 Å in the 4 and 5 central thiophene rings is also apparent. For this species, the central inter-ring bond shortens from 1.439 Å in the neutral species to 1.392 Å in the dicationic form, so the quinonoid character is larger than in the radical cation species. The end-phenyl caps in $Ph_2Me_4SxT^{2+}$ are slightly affected by the doubly ionization: the CC bonds that connect the thiophene rings with the phenyl rings only change from 1.466 Å in the neutral form to 1.449 Å (1.461 Å in the radical cation).

Further ionization of $Ph_2Me_4SxT^{2+}$ to $Ph_2Me_4SxT^{3+\cdot}$ produces larger changes for the end-phenyl groups: the lengths of the CC bond numbers 2 and 3 change 0.01 and 0.02 Å, respectively (Figure 3c); while on going from the neutral to the dication species they scarcely change. The optimized geometry of $Ph_2Me_4SxT^{3+\cdot}$ shows a reversed bond length alternation pattern (average value of 0.04 Å) or quinonoid structure that is extent over all the thiophene rings.

For the tetracation, $Ph_2Me_4SxT^{4+}$, the trend established for $Ph_2Me_4SxT^{3+\cdot}$ is also observed (Figure 3d). The quinonoid character is strongly marked in the phenyl groups: the lengths

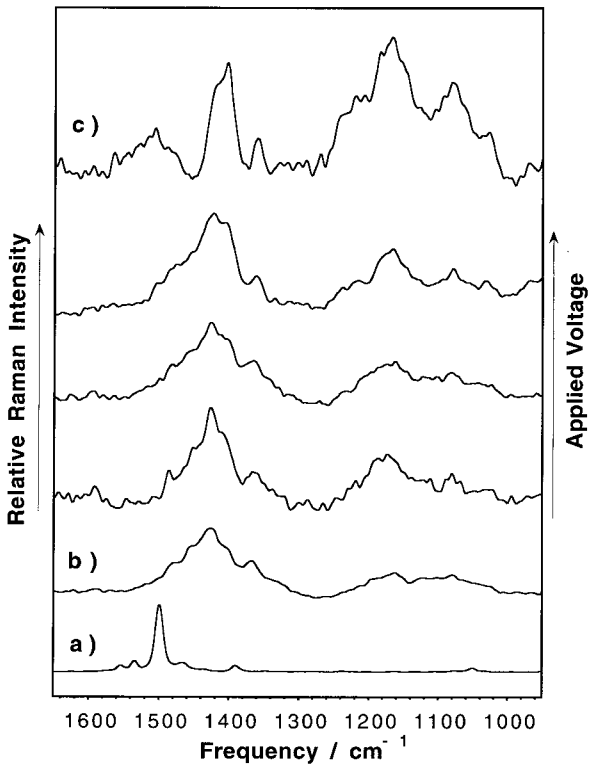

Figure 4. FT-Raman spectra over probe energies of 1700−1000 cm^{-1} recorded during the electrochemical oxidation of Me_2Bu_4SxT. (a) Neutral molecule (solid state), (b) first oxidation process, and (c) second oxidation process. Unlabeled spectra correspond to intermediate voltages.

of the CC bond numbers 2 and 3 change by 0.015 Å and by 0.03 Å, respectively. However, the quinonoid character in the innermost part of the molecule is weaker than in the case of the less ionized species.

The analysis of the Mulliken atomic charges supports some of the experimental results concerning the stability of the highest oxidized species in Me_2Bu_4SxT and in Ph_2Bu_4SxT. The total positive charge over each of the end-phenyl groups are $+0.01e$ in Ph_2Me_4SxT, $+0.10e$ in $Ph_2Me_4SxT^{+\cdot}$, $+0.26e$ in $Ph_2Me_4SxT^{2+}$, $+0.46e$ in $Ph_2Me_4SxT^{3+\cdot}$, and $+0.61e$ in $Ph_2Me_4SxT^{4+}$. In the case of the $Ph_2Me_4SxT^{3+\cdot}$, the phenyl groups support almost one positive charge, with two positive charges supported by the thiophene backbone. For $Ph_2Me_4SxT^{4+}$, the phenyl groups support 1.22 positive charges and the thiophene backbone must support 2.78 positive charges. Since previous results show that only a dication species is stable in the case of α,α′-alkyl end-capped sexithiophene,[30] these theoretical results demonstrate that the two phenyl end-cap groups have a decisive role in stabilizing the radical trication and the tetracation species and suggest that the butyl groups are also stabilizing the highly charged species.

IV. Spectroelectrochemical Raman Study of Me_2Bu_4SxT

Some of us have previously reported on the Raman spectra of α,α-dimethyl sexithiophene (Me_2SxT).[16,31] The most intense Raman bands for the neutral (1477 cm^{-1}), cation radical (1437 cm^{-1}) and dication (1415 cm^{-1}) were assigned to the ECC mode. Similar spectra and shifts were measured for Me_2Bu_4SxT (Figure 4). The Raman spectrum of the neutral Me_2Bu_4SxT has the most intense band at 1499 cm^{-1}; on the other hand, the electrochemically generated cation radical shows the strongest Raman band at 1426 cm^{-1} and the dication at 1408 cm^{-1}.

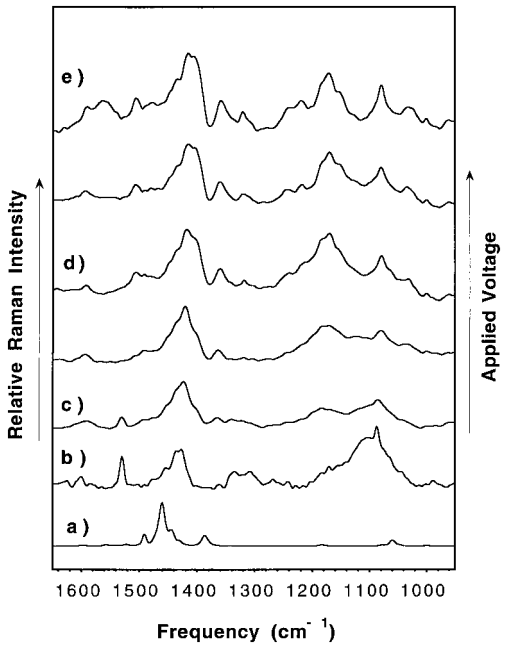

Figure 5. FT-Raman spectra over probe energies of 1700−1000 cm^{-1} recorded during the electrochemical oxidation of Ph_2Bu_4SxT. (a) neutral molecule (solid state), (b) first oxidation process, (c) second oxidation process, (d) third oxidation process, and (e) fourth oxidation process. Unlabeled spectra correspond to intermediate voltages.

In Me_2Bu_4SxT, the band at 1167 cm^{-1} strongly increases its intensity upon oxidation. A similar increase has been recently found in the case of an α,α′-dithiohexyl sexithiophene: the band at 1157 cm^{-1} becomes almost the strongest of the dication spectrum of this molecule.[32] Similarly for Ph_2Bu_4SxT the band at 1167 cm^{-1} strongly increases in intensity when oxidized (see below).

V. Spectroelectrochemical Vibrational Study of Ph_2Bu_4SxT

V.a. In Situ Spectrolectrochemical Raman Results. Figure 5 shows the Raman spectra of Ph_2Bu_4SxT as a function of the applied voltage and the Raman spectrum of the neutral material, and Table 1 summarizes the frequency values of the most important bands.

The Raman spectrum of species generated at low voltages shows bands at 1437 cm^{-1} and 1426 cm^{-1}. We assign the 1437 cm^{-1} band to the radical cation ($Ph_2Me_4SxT^{+\cdot}$). This assignment agrees with a previous one for the radical cation of diphenyl-terthiophene (1438 cm^{-1}) and the DFT calculated spectrum for $Ph_2Me4SxT^{+\cdot}$ (1430 and 1389 cm^{-1}). The band at 1426 cm^{-1} is assigned to the dication ($Ph_2Bu_4SxT^{2+}$). This assignment is consistent with the DFT calculated spectrum for $Ph_2Me_4SxT^{2+}$ (1393 cm^{-1}) and with the Raman spectrum of the dication species of diphenyl-tetrathiophene (1430−1427 cm^{-1}).[33] Importantly, further oxidation leads to enhancement of the bands we have assigned to the dication. It is noted that although the radical cation (λ_{max} at 811 and 1373 nm) is off resonance, the dication (λ_{max} at 1155 nm) is on resonance and so its spectrum is dramatically enhanced.[34] This explains obtaining spectra of the dication even at low concentration in mixture with the cation radical.

At higher voltages, the Raman band of the dication ($Ph_2Bu_4SxT^{2+}$) species at 1426 cm^{-1} clearly appears and is then progressively replaced by a band at 1415 cm^{-1}. The band at 1415 cm^{-1} is assigned to the radical trication, $Ph_2Bu_4SxT^{3+}$. As in the case of the dication, the Raman spectrum of the radical

TABLE 1: Correlation between the Frequencies of the Main Bands Recorded in the Raman Spectra of the Neutral Ph_2Bu_4SxT (Solid State) and of Its Oxidized Species (in 0.1 M $TBABF_6$ in CH_2Cl_2): Radical Cation ($Ph_2Bu_4SxT^{+\cdot}$), Dication ($Ph_2Bu_4SxT^{2+}$), Radical Trication ($Ph_2Bu_4SxT^{3+\cdot}$), and Tetracation ($Ph_2Bu_4SxT^{4+}$)[a]

Ph_2Bu_4SxT	$Ph_2Bu_4SxT^{+\cdot}$	$Ph_2Bu_4SxT^{2+}$	$Ph_2Bu_4SxT^{3+\cdot}$	$Ph_2Bu_4SxT^{4+}$	assignment
1600 (1641)		1593 (1624)	1592 (1619)	1591 1563	ν(C=C)$_{phenyl}$
1520 1491 (1483)	1530	1508	1506 (1517)	1506	**line A**
1459 (1446) 1444	**1437** (1430) **1426** (1389)	**1426** (1393)	**1415** (1406)	1403*sh* (1420)	**line B** **line C**
1387 (1378)		1365 (1360−1340)	1365	1360 (1353) 1221	$\delta(CH_2)$
		1170 (1193)	1170 (1215)	1172 (1227)	δ(CCH)
1060 (1046)					**line D**

[a] In parentheses, the corresponding B3LYP/3-21G theoretical frequencies calculated in Ph_2Me_4SxT are shown. In bold, the most intense band.

trication is taken in resonant Raman conditions because of its electronic absorption band at 1160−990 nm.

The Raman spectra at the highest voltages show an important shoulder at 1403 cm^{-1} that increases in intensity with voltage. However, it does not become the strongest band of the spectrum. This new Raman band is tentatively assigned to the fourth one-electron oxidized species, $Ph_2Bu_4SxT^{4+}$. A well-resolved Raman spectrum for the tetracation is not recorded because of its lack of stability on the time scale of the Raman experiment, and because the Raman spectrum of this species is taken in preresonant Raman conditions with the electronic absorption at 966 nm.

V.b. Assignment of the Raman Bands. The theoretical B3LYP/3-21G* Raman spectra of the neutral, radical cation, dication, radical trication, and tetracation species of Ph_2Me_4SxT together with the corresponding experimental features of Ph_2Bu_4SxT are shown in Figure 6 and in Figure 6S (in the Supporting Information). Figure 7 depicts the corresponding eigenvector associated to the most intense band of either the neutral theoretical Raman spectrum and each oxidized species.

The B3LYP/3-21G* Raman spectrum of the neutral Ph_2Me_4SxT reproduces quite well the experimental spectrum. The most intense Raman band is calculated at 1446 cm^{-1} that we correlate with the experimental band at 1459 cm^{-1} and assign to the ECC mode on the basis of its theoretical eigenvector (Figure 7).

This 1459 cm^{-1} band is mainly made up of intra-ring C−C, C=C, and C−S stretching components. Upon oxidation, the values of the force constants of the C=C stretching components decrease and those of the C−C bonds increase significantly with a net decrease in the frequency associated with this mode. The UB3LYP/3-21G* theoretical Raman spectrum of $Ph_2Me_4SxT^{+\cdot}$ shows the most intense Raman bands at 1430 cm^{-1} and at 1389 cm^{-1}. We correlate the experimental band of the radical cation at 1437 cm^{-1} with the theoretical band at 1430 cm^{-1}. Due to the resemblance of its associated eigenvector with that of the 1459 cm^{-1} band in neutral Ph_2Me_4SxT, it is assigned to the ECC mode of the radical cation (Figure 7). Theoretical calculations show that the two inner thiophene rings acquire a quinonoid pattern, so the strongest Raman band shifts down to 1437 cm^{-1}.

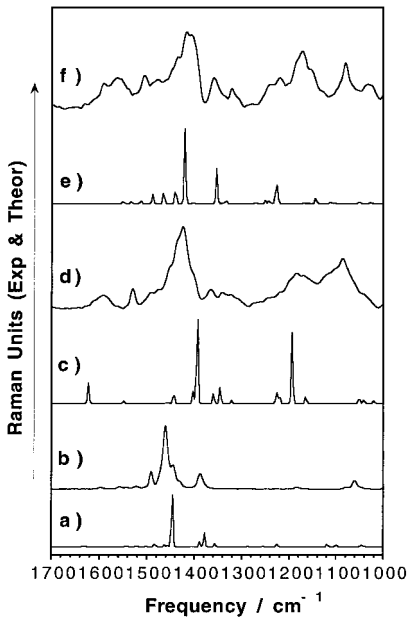

Figure 6. Comparison between the theoretical B3LYP/3-21G* Raman spectra of (a) neutral, (c) dication, and (e) tetracation species of Ph_2Me_4SxT, and of the experimental Raman spectra of (b) neutral, (d) dication, and (f) tetracation species of Ph_2Bu_4SxT.

The B3LYP/3-21G* Raman spectrum of $Ph_2Me_4SxT^{2+}$ predicts the existence of an intense Raman dispersion at 1393 cm^{-1} (ECC mode) correlated with the experimental Raman band of $Ph_2Me_4SxT^{2+}$ at 1426 cm^{-1}, as well as a band at 1193 cm^{-1}. For the dication species, the quinonoid pattern is extended over 4−5 thiophene rings and, as expected, a larger decrease in the Raman frequency of the ECC mode occurs than that in the radical cation.

The quinonoid pattern reaches the phenyl groups in the radical trication species, but the quinonoid character is still strongly

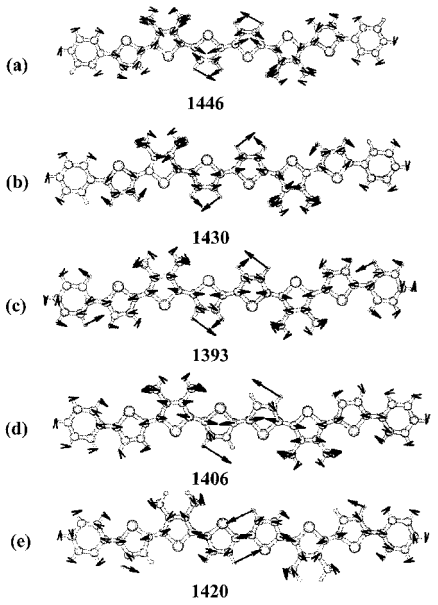

Figure 7. Schematic eigenvectors associated to the most intense Raman bands of the spectra of the (a) neutral, (b) radical cation, (c) dication, (d) radical trication, and (e) tetracation species of Ph_2Me_4SxT. The B3LYP/3-21G* and UB3LYP/3-21G* methods have been used for the closed-shell and for the open-shell systems, respectively.

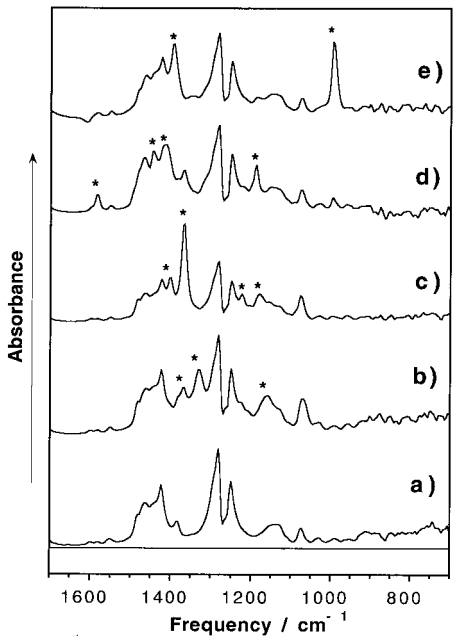

Figure 8. FT-infrared spectra over probe energies of 1700−700 cm^{-1} recorded during the electrochemical oxidation of Ph_2Bu_4SxT. (a) first oxidation process, (b) second oxidation process, (c) third oxidation process, and (d) fourth oxidation process. Asterics correspond to bands of Ph_2Bu_4SxT; the rest of bands arise from the electrolite.

marked in the four outermost thiophene rings. The calculated Raman spectrum of $Ph_2Me_4SxT^{3+}$ is satisfactorily similar to the experimental spectrum and predicts the most intense band at 1406 cm^{-1} that is correlated with the experimental feature at 1415 cm^{-1} corresponding again to the ECC mode of this species.

Finally, theoretical calculations carried out in $Ph_2Bu_4SxT^{4+}$ show that the quinonoid pattern is extended over the entire molecule and the quinonoid character of the thiophene backbone increases even with respect to the radical trication. The B3LYP/3-21G Raman spectrum of $Ph_2Bu_4SxT^{4+}$ shows the most intense band at 1420 cm^{-1} that we correlate with the experimental one at 1403 cm^{-1}. Once again, the ECC mode downshifts in frequency with respect to the radical trication in agreement with the further extension of the quinonoid character.

The experimental Raman data for the bands near 1400 cm^{-1} (Table 1) show a decrease in frequency with each increased level of oxidation. The theoretical results, although useful in the assignment of these bands, do not show such a good correlation. Producing accurate values for Raman frequencies for such a large number of oxidation states in such complex molecules is no simple theoretical task. It is especially daunting since two of the species are open shell. We chose not to use any scaling factors for these calculations. If different scaling factors were used for each species we would improve the quality of the frequencies obtained, and we feel confident that the correlation would improve.

The Raman spectrum of the neutral Ph_2Bu_4SxT has a band at 1600 cm^{-1} assigned to a ν(C═C) vibration of the phenyl groups in basis of the eigenvector associated to the theoretical Raman band at 1641 cm^{-1}. This vibration also changes its frequency as a function of the oxidation state as is expected from the theoretical calculations. In the Raman spectra of the oxidized species of Ph_2Bu_4SxT a downshift from 1600 cm^{-1} in the neutral species to 1592 cm^{-1} in the trication radical is observed. However, the most significantly changes of the phenyl ν(C═C) frequency occurs in $Ph_2Bu_4SxT^{4+}$ where it is measured at 1563 cm^{-1}. These results are in agreement with previously results in PPV.[16,35] In this polymer the phenyl ν(C═C) frequency downshifts from 1582 cm^{-1} in the neutral material to 1568 cm^{-1} in an oxidized polymer.

The band around 1170 cm^{-1} increases its intensity when oxidation level increases. This band should be correlate with the theoretical features at 1193 cm^{-1} in the dication species, 1215 cm^{-1} in the radical trication and 1227 cm^{-1} in the tetracation, and could be described like an CCH bending vibration of the phenyl rings.[16,35] The increase of its intensity could be justified by the fact that the ionization affects to the phenyl groups mainly at higher oxidation levels. This vibration is coupled with the ν(C−C) and with the δ(C−H) vibrations of the side chains. Probably, the large number of ν(C−C) and δ(C−H) vibrations, due to the four butyl chains, involved in this normal mode could also justify the large intensity of its associated Raman band.

The band at 1387 cm^{-1} in the neutral material is assigned to an $\delta(CH_2)$ vibration of the butyl chains strongly coupled with the ECC mode. When oxidation progresses, the charge defect is extended over the entire molecule and the $\delta(CH_2)$ vibrations couple with the C═C/C−C stretching vibrations of the electronic defect what could justify the medium intensity of its associated Raman band.

V.c. In Situ Infrared Spectroelectrochemical Study. Figure 8 shows the infrared spectra recorded during the electrochemical oxidation of the Ph_2Bu_4SxT, and Table 2 summarizes the frequency values of the most important bands. The theoretical B3LYP/3-21G* infrared spectra of the neutral, radical cation, dication, radical trication, and tetracation species of Ph_2Me_4SxT together with the corresponding experimental features of Ph_2Bu_4SxT are shown in Figure 9 and in Figure 9S (in the Supporting Information). Figure 10 depicts the corresponding eigenvector associated to the most intense band of the theoretical IR spectra of the oxidized species. The analysis of the IR features during the electrochemical oxidation is difficult due to the large number of bands appearing in the spectral region from 1700 to 1000 cm^{-1} including those of the solvent and electrolyte. Nevertheless, the changes of the most

TABLE 2: Correlation between the Frequencies of the Main IR Bands of the Neutral Ph_2Bu_4SxT (solid state) and of Its Oxidized Species (in 0.1 M $TBABF_6$ in CH_2Cl_2): Radical Cation ($Ph_2Bu_4SxT^{+\cdot}$), Dication ($Ph_2Bu_4SxT^{2+}$), Radical Trication ($Ph_2Bu_4SxT^{3+\cdot}$), and Tetracation ($Ph_2Bu_4SxT^{4+}$)[a]

Ph_2Bu_4SxT	$Ph_2Bu_4SxT^{+\cdot}$	$Ph_2Bu_4SxT^{2+}$	$Ph_2Bu_4SxT^{3+\cdot}$	$Ph_2Bu_4SxT^{4+}$	assignment
1596 (1630)			1587 (1615)	1582 (1622)	ν**(C=C)$_{phenyl}$**
1486 (1542)					ν_s**(C=C)**
			1467 (1443)		
1458 (1515)					ν_a**(C=C)**
		1401 (1404)			
	1368 **1330** (1373)	**1365** (1396)	**1412** (1370)	**1394** (1372)	**ν(CC)**
		1222 (1237) 1180 (1217)			
	1158 (1222)				
				1041	
793 (786) 751					**γ(CH)**

[a] In parenthesis, the corresponding B3LYP/3-21G theoretical frequencies calculated in Ph_2Me_4SxT are shown. In bold, the most intense band.

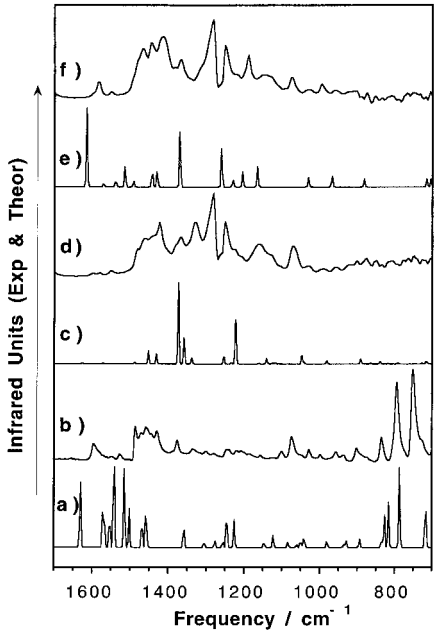

Figure 9. Comparison between the theoretical B3LYP/3-21G* infrared spectra of (a) neutral, (c) dication, and (e) tetracation species of Ph_2Me_4SxT and of the experimental infrared spectra of (b) neutral, (d) dication, and (f) tetracation species of Ph_2Bu_4SxT.

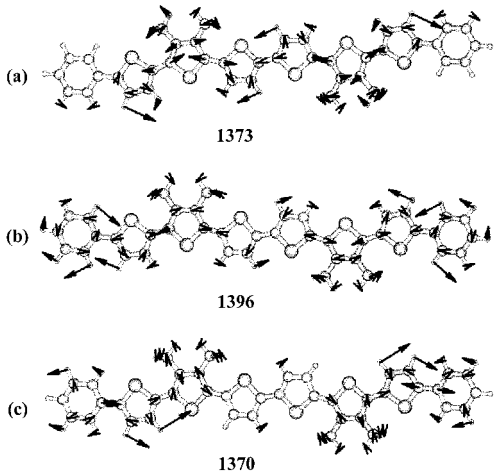

Figure 10. Schematic eigenvectors associated to the most intense IR bands of the spectra of (a) radical cation, (b) dication, and (c) radical trication species of Ph_2Me_4SxT. The B3LYP/3-21G* and UB3LYP/3-21G* methods have been used for the closed-shell and for the open-shell systems, respectively.

intense bands on going from the lower to the higher oxidation potentials will be reported.

The effects of oxidation on the infrared spectra of oligothiophenes have been studied.[14] The computed dipole moment derivatives with respect to the internal coordinates show that the largest contributions to the IR intensities in the oxidized materials stem from CC bond stretching vibrations. Of them, the dipole moment derivatives with respect to the CC bonds located on the defects (quinonoid pattern) only show small contributions. The largest contributions to the IR intensities stem from CC bonds located in the transition region from benzenoid to quinonoid patterns. These vibrations cannot be assigned to the displacements of any individual bond or angle, but are coupled with ν(C−C) inter-ring vibrations of the quinonoid structure.[14,15]

With these theoretical results as a guide, it is possible to understand the evolution of the most intense infrared bands with oxidation state. An intense IR band for the radical cation appears at 1330 cm^{-1}, dication at 1365 cm^{-1}, radical trication at 1412 cm^{-1} and tetracation at 1394 cm^{-1}. Optimized geometries show

that the transition region from the quinonoid to the benzenoid patterns are clearly shown in the case of the $Ph_2Bu_4SxT^{+\cdot}$, $Ph_2Bu_4SxT^{2+}$, and $Ph_2Bu_4SxT^{3+\cdot}$. We correlate the experimental bands at 1330, 1365, and 1412 cm^{-1} with the most intense infrared band of the spectrum of $Ph_2Me_4SxT^{+\cdot}$ at 1373 cm^{-1}, $Ph_2Bu_4SxT^{2+}$ at 1396 cm^{-1}, and $Ph_2Me_4SxT^{3+\cdot}$ at 1370 cm^{-1}, respectively. In basis of their associated eigenvectors we should described these vibrations as ν(C−C) vibrations with large contributions from the ν(C−C) located in the transition region. The normal modes associated with these intense bands have an important contribution from the inter-ring ν(C−C) vibrations of the quinonoid structure, and these bonds are strengthened after oxidation. The strengthening of the inter-ring bonds is consistent with the frequency increase of the most intense IR bands.

For $Ph_2Bu_4SxT^{3+\cdot}$, the transition region is partially located in the phenyl groups, and one infrared band at 1587 cm^{-1}, assigned to phenyl ν(C−C) vibrations, is observed (theoretical band at 1615 cm^{-1}). In $Ph_2Bu_4SxT^{4+}$, the transition region is not clearly predicted by the theoretical calculations as the quinonoid structure is dominant throughout. This result is consistent with the small IR intensity and frequency of the most intense IR band in $Ph_2Bu_4SxT^{4+}$ with respect to those of $Ph_2Bu_4SxT^{2+}$ and $Ph_2Bu_4SxT^{3+\cdot}$.

VI. Conclusions

Two sexithiophene molecules bearing solublizing alkyl groups and terminally substituted with phenyl and methyl groups have been characterized by infrared and Raman spectroscopies. Extensive quantum chemical calculations of the equilibrium structures of the radical cation, dication, radical trication, and tetracation of Ph_2Me_4SxT at the B3LYP/3-21G level were performed to support these results. The combination of the DFT calculations with the theoretical formalism of the ECC theory has yielded a satisfactory explanation of the changes observed in the Raman spectra of the oxidized materials.

The present study shows that in situ vibrational spectroscopy combined with modern theory is a powerful tool to characterize the structures in highly oxidized oligothiophenes. It is shown how the charges are delocalized, and how the phenyl end groups stabilize the four oxidized species. The spectra and calculations give insight into the modes of charge delocalization in these species, which would be otherwise obscure.

This paper documents several advances: (1) IR and Raman spectra for 5 different oxidation states of one molecule, (2) correlation of vibrational shifts for these species, (3) the use of DFT calculations to understand these spectra, and (4) the utility of spin unrestricted basis sets to correlate vibrational spectra of radical cations and radical trications. To our knowledge, this work presents for the first time the Raman spectra of higher oxidized species than a dication.

Acknowledgment. The present work was supported in part by the Dirección General de Enseñanza Superior (DGES, MEC, Spain) through the research projects FD97-1765-C03 and BQU2000-1156. We are also indebted to Junta de Andalucía (Spain) for funding for our research group (FQM-0159). J.C. is grateful to the Ministerio de Educacion y Cultura of Spain for a PostDoctoral fellowship at the University of Minnesota (Formación y Perfeccionamiento de Doctores y Tecnólogos en el Extranjero, referencia PF00 25327895). Work at the University of Minnesota was supported by the National Science Foundation.

Supporting Information Available: Figure 6S showing the theoretical B3LYP/3-21G* Raman spectra of the neutral, radical cation, and radical trication species of Ph_2Me_4SxT together with the corresponding experimental features of Ph_2Bu_4SxT. Figure 9S showing the theoretical B3LYP/3-21G* infrared spectra of the neutral, radical cation, and radical trication species of Ph_2Me_4SxT together with the corresponding experimental features of Ph_2Bu_4SxT. This material is available free of charge via the Internet at http://pubs.acs.org.

References and Notes

(1) Elsenbaumer, R. L., Skotheim, T., Reynolds, J. R., Eds. *Handbook of Conductive Polymers*; Dekker: New York, 1998. Nalwa, H. S., Ed. *Handbook of Organic Conductive Molecules and Polymers*; John Wiley & Sons: Chichester, 1997.

(2) Mullen, K., Wegner, G., Eds. *Electronic Materials: The Oligomer Approach*; ; Wiley-VCH: Weinheim, 1997. *Handbook of Oligo- and Polythiophenes*; Fichou, D., Eds.; Wiley-VCH: Weinheim, 1999.

(3) Roncali, J. *Chem. Rev.* **1997**, *97*, 173.

(4) Graf, D. D.; Campbell, J. P.; Mann, K. R.; Miller L. L. *J. Am. Chem. Soc.* **1996**, *118*, 5480. Graf, D. D.; Duan, R. G.; Campbell, J. P.; Miller, L. L.; Mann, K. R. *J. Am. Chem. Soc.* **1997**, *119*, 5888. Bauerle, P.; Segelbacher, U.; Maier, A.; Mehring, M. *J. Am. Chem. Soc.* **1993**, *115*, 10217. Bauerle, P.; Fisher, T.; Bidlingmeier, B.; Stabel, A.; Rabe, J. *Angew. Chem., Int. Ed. Engl.* **1995**, *34*, 303.

(5) Kromer J.; Rios-Carreras I.; Fuhrmann G.; Musch C.; Wunderlin M.; Debaerdemaeker T.; Mena-Osteritz E.; Bauerle P. *Angew. Chem. Int. Ed.* **2000**, *39*, 3481. Funaoka, S., Imae, I., Noma, N., Shirota, Y. *Synth. Met.* **1999**, *101*, 600.

(6) Jestin, I.; Frere, P.; Mercier, N.; Levillain, E.; Stievenard, D.; Roncali, J. *J. Am. Chem. Soc.* **1998**, *120*, 8150. Elandaloussi, E. H.; Frere, P.; Richomme, P.; Orduna, J.; Garin, J.; Roncali, J. *J. Am. Chem. Soc.* **1997**, *119*, 10774.

(7) van Haare, J. A. E. H.; Havinga E. E.; van Dongen J. L. J.; Janssen R. A. J.; Cornil J.; Bredas J. L. *Chem. Eur. J.* **1998**, *4*, 1509. van Haare J. A. E. H.; van Boxtel M.; Janssen R. A. J. *Chem. Mater.* **1998**, *10*, 1166.

(8) Bauerle, P.; Segelbacher, U.; Gaudl, K.-L.; Huttenlocher, D.; Mehring, M. *Angew. Chem., Int. Ed. Engl.* **1993**, *32*, 76.

(9) Parakka, J. P.; Jeevarajan, J. A.; Jeevarajan, A. S.; Kispert, L. D.; Cava, M. P. *Adv. Mater.* **1996**, *8*, 54. Noda, T.; Imae, I.; Noma, N.; Shirota, Y. *Adv. Mater.* **1997**, *9*, 239. Noda, T.; Ogawa, H.; Noma, N.; Shirota, Y. *Adv. Mater.* **1997**, *9*, 720.

(10) Jestin, I.; Frere, P.; Levillain, E.; Roncali, J. *Adv. Mater.* **1999**, *11*, 134.

(11) Pappenfus, T. M.; Hukkanen, E. J.; Graf, D. D.; Mann, K. R. *Chem. Mater.* Submitted for publication.

(12) Zerbi, G.; Gussoni, M.; Castiglioni, C. *Conjugated Polymers*; Bredas, J.-L., Silbey, R., Eds.; Kluwer Academic Publishers: Dordrecht, The Nethelands, 1991, 435. Del Zoppo, M.; Castiglioni, C.; Zuliani, P.; Zerbi, G.; in *Handbook of Conductive Polymers*; Elsenbaumer, R. L., Skotheim, T., Reynolds, J. R., Eds.; Dekker: New York, 1998; p 765.

(13) Furukawa, Y.; Ohtsuka, H.; Tasumi, M. *Synth. Met.* **1993**, *55*−*57*, 516. Sakamoto, A.; Furukawa, Y.; Tasumi, M. *J. Phys. Chem.* **1992**, *96*, 3870. Yokonuma, N.; Furukawa, Y.; Tasumi, M. Kuroda, M.; Nakayama, J.; *Chem. Phys. Lett.* **1996**, *255*, 431. Furukawa, Y. *J. Phys. Chem.* **1996**, *100*, 15645.

(14) Cuff, L.; Chagxing, C.; Kertesz, M. *J. Am. Chem. Soc.* **1994**, *116*, 9269. Choi, C. H.; Kertesz, M.; Mihaly, L. *J. Phys. Chem.* **2000**, *104*, 102.

(15) Louarn, G.; Buisson, J.-P.; Lefrant, S.; Fichou, D. *J. Phys. Chem.* **1995**, *99*, 11399. Baitoul, M.; Wery, J.; Buisson, J.-P.; Arbuckle, G.; Shah, H.; Lefrant, S.; Handoume, M. *Polymer* **2000**, *41*, 6955.

(16) Casado, J.; Hernandez, V.; Hotta, S.; Lopez Navarrete, J. T. *Adv. Mater.* **1998**, *10*, 1458. Casado, J.; Hernandez, V.; Hotta, S.; Lopez Navarrete, J. T. *J. Chem. Phys.* **1998**, *109*, 10419.

(17) Castiglioni, C.; Lopez Navarrete, J. T.; Gussoni, M.; Zerbi, G. *Solid State Commun.* **1988**, *65*, 625. Zerbi, G.; Castiglioni, C.; Lopez Navarrete, J. T.; Tian, B.; Gussoni, M. *Synth. Met.* **1989**, *28*, D359.

(18) Labanowski, J. K.,. Andzelm, J. W., Eds. *Density Functional Methods in Chemistry*; Springer: New York, 1991.

(19) Koch, W.; Holthausen, M. C. *A Chemist's Guide to Density Functional Theory*, 2nd ed.; Wiley-VCH: Weinheim, 2001.

(20) Furuya, K.; Torii, H.; Furukawa, Y.; Tasumi, M. *J. Mol. Struct. (THEOCHEM)* **1998**, *424*, 225.

(21) Hernandez, V.; Calvo Losada, S.; Casado, J.; Higuchi, H.; Lopez Navarrete, J. T. *J. Phys. Chem. A* **2000**, *104*, 661. Hernandez, V.; Casado, J.; Effenberger, F.; Lopez Navarrete, J. T. *J. Chem. Phys.* **2000**, *112*, 5105.

(22) Parente, V.; Pourtois, G.; Lazzaroni, R.; Bredas, J. L.; Ruani, G.; Murgia, M.; Zamboni, R. *Adv. Mater.* **1998**, *10*, 319.

(23) Frisch, M. J.; Trucks, G. W.; Schlegel, H. B.; Scuseria, G. E.; Robb, M. A.; Cheeseman, J. R.; Zakrzewski, V. G.; Montgomery, J. A.; Stratman,

R. E.; Burant, S.; Dapprich, J. M., Millam, J. M.; Daniels, A. D.; Kudin, K. N.; Strain, M. C.; Farkas, O.; Tomasi, J.; Barone, V.; Cossi, M.; Cammi, R.; Mennucci, B.; Pomelli, C.; Adamo, C.; Clifford, S.; Ochterski, G.; Petersson, A.; Ayala, P. Y.; Cui, Q.; Morokuma, K.; Malick, D. K.; Rabuck, A. D.; Raghavachari, K.; Foresman, J. B.; Cioslowski, J.; Ortiz, J. V.; Stefanov, B. B.; Liu, G.; Liashenko, A.; Piskorz, I.; Komaromi, I.; Gomperts, R.; Martin, R. L.; Fox, D. J.; Keith, T.; Al-Laham, M. A.; Peng, C. Y.; Manayakkara, A.; Gonzalez, C.; Challacombe, M.; Gill, P. M. W.; Johnson, B. G.; Chen, W.; Wong, M. W.; Andres, J. L.; Head-Gordon, M.; Replogle, E. S.; Pople, J. A. *Gaussian 98*, revision A.1; Gaussian, Inc.: Pittsburgh, PA, 1998.

(24) Becke, A. D. *J. Chem. Phys.* **1993**, *98*, 5648.

(25) Viruela, P.; Viruela, R.; Orti, E.; Bredas, J. L. *J. Am. Chem. Soc.* **1997**, *119*, 1360.

(26) Scott, A. P.; Radom, L. *J. Phys. Chem.* **1996**, *100*, 16502.

(27) Rauhut, G.; Pulay, P. *J. Phys. Chem.* **1995**, *99*, 3093.

(28) Francl, M. M.; Pietro, W. J.; Hehre, W. J.; Binkley, J. S.; Gordon, M. S.; Defrees, D. J.; Pople, J. A. *J. Chem. Phys.* **1982**, *77*, 3654.

(29) Cuff, L.; Miklos, K. *J. Chem. Phys.* **1997**, *106*, 5541.

(30) Zotti, G.; Schiavon, G.; Berlin, A.; Pagani, G. *Chem. Mater.* **1993**, *5*, 430. Zotti, G.; Schiavon, G.; Berlin, A.; Pagani, G. *Chem. Mater.* **1993**, *5*, 620. Casado, J.; Bengoechea, M.; Lopez Navarrete, J. T.; Otero, T. F. *Synth. Met.* **1998**, *95*, 93.

(31) Hernandez, V.; Casado, J.; Ramirez, F. J.; Zotti, G.; Hotta, S.; Lopez Navarrete, J. T. *J. Chem. Phys.* **1996**, *104*, 9271; Ramirez, F. J.; Aranda, M. G. A.; Hernandez, V.; Casado, J.; Hotta, S.; Lopez Navarrete, J. T. *J. Chem. Phys.* **1998**, *109*, 1920. Casado, J.; Hotta, S.; Hernandez, V.; Lopez Navarrete, J. T. *J. Phys. Chem. A.* **1999**, *103*, 816.

(32) Casado, J.; Katz, H. E.; Hernandez, V.; Lopez Navarrete, J. T. *Mater. Res. Soc. Symp.* **2001**, *660*.

(33) Casado, J.; Hernandez, V.; Hotta, S.; Lopez Navarrete, J. T. *Synth. Met.* **2001**, *119*, 305.

(34) Albrecht, C. A. *J. Chem. Phys.* **1961**, *34*, 1476.

(35) Froyer, G.; Simmonneau, A.; Buisson, J.-P.; Mevellec, J. Y.; Lefrant, S. *J. Phys. Chem. A* **1999**, *103*, 7625.